Scanning Microscopy Vol. 12, No. 2, 1998 (Pages 265-284) 0891-7035/98$5.00+.25
Scanning Microscopy International, Chicago (AMF O'Hare), IL 60666 USA

NON LINEAR EFFECTS IN ION INDUCED ELECTRON EMISSION

G. Schiwietz[1]*, G. Xiao[2], P.L. Grande[3], A. Schmoldt[1], M. Grether[1], R. Köhrbrück[1], A. Spieler[1] and U. Stettner[1]

[1]Hahn-Meitner-Institut Berlin GmbH, Bereich Festkörperphysik, Berlin, Germany; [2]DAAD fellow;
[3]Instituto de Física, Universidade Federal do Rio Grande do Sul, BR-91500 Porto Alegre, Brazil

(Received for publication May 11, 1996 and in revised form January 21, 1997)

Abstract

High-resolution zero-degree electron spectra, total electron yields as well as Auger-electron spectra have been taken for 5 MeV/u ions (N^{7+}, S^{13+}, Ni^{23+}, and Ag^{37+}) penetrating carbon and insulator foils at normal incidence. A shift of the convoy-electron velocity with respect to the experimentally determined projectile velocity is found. For the carbon target, there is an acceleration of convoy electrons, whereas for the insulating targets, there is a deceleration of convoy-electrons as well as a deceleration of target-Auger electrons. These experimental findings are compared to theoretical estimates for dynamic ion-induced potentials.

Key Words: Electron yields, Auger spectra, convoy electrons, non-linear effects, nuclear-track potential, electron recombination, image potential, Coulomb explosion.

*Address for correspondence:
G. Schiwietz
Hahn-Meitner-Institut Berlin GmbH
Bereich Festkörperphysik
Glienicker Str. 100
D-14109 Berlin, Germany
Telephone number: +49-30-8062-2448
E-mail: schiwietz@hmi.de

Introduction

Ion-solid interactions have been investigated for more than a century [50]. Two different categories of investigations may be distinguished: those that are concerned with the influence of the target on the **projectile** state including its motion, and those that determine the influence of the projectile on static and dynamic properties of the **solid**. The first category includes the determination of stopping powers, angular and energy straggling [2, 5, 10, 13, 16, 17, 37, 41, 46, 47, 55, 58, 69, 72, 73, 91, 94, 95, 101, 123] as well as projectile charge-states and specific state populations [4, 11, 12, 18, 29, 30, 77, 85, 86, 90, 114, 122; also, private communication with Y. Yamazaki and N. Stolterfoht, 1994]. Many of these projectile-related quantities are well described and understood, especially for fast ions. In the second category, transient material states and permanent modifications of bulk or surface properties of solids are examined. Although the underlying basic atomic mechanisms have been investigated intensively, there is still a considerable lack of information concerning the properties of a highly excited solid. The large body of experimental and theoretical works, for mainly singly-charged projectiles, suggests a distinction between nuclear and electronic damage-production/rearrangement mechanisms. Especially the electronic excitations are often sensitive to details of the target structure, and these electronic mechanisms govern the ion-solid interaction for fast projectiles.

The main unsolved question concerning material modifications is how the electronic excitations are converted into atomic motion. The Coulomb-explosion model [42, 62, 109, 117] is based on the assumption that target atoms get ionized (or excited in similar models), and electron recombination is slow enough, so that mutual atomic repulsion can take place. Thus, the electronic potential energy, or equivalently, the degree of target ionization/excitation, leads to the atomic motion in this model. The thermal-spike model [66, 79, 109, 116] assumes that electronic excitation leads, via the electron-photon coupling, directly to an atomic motion. Thus, except for the electron-photon coupling, the kinetic electron energy is the main ingredient in this model. It is

emphasized, however, that atomic motion in solid matter will be converted into a stochastic motion on a time scale of 10^{-13} to 10^{-12} s (s = seconds), independent of the early stage of evolution. Hence, there seems to be no way to decide between both models on a pure experimental basis, if only macroscopic properties are investigated.

One possible way to improve the interpretation of material modification effects is the investigation of prompt emitted "particles" that carry information from inside the track. Ejected electrons or X-rays can be used as precursors of the corresponding transient material states. Electrons may be probes for the first 10^{-17} to 10^{-14} s of the track formation and energy dissipation. For reviews on transport of fast electrons and fast-ion-induced electron emission from solids, see [14, 53, 82, 84, 92]. The continuous part of the electron spectrum will be referred to as δ-electrons or secondary electrons (in the sense of secondary particles) throughout this paper.

In this paper, we will be concerned with projectiles at energies of 5 MeV/u, corresponding to 10% of the speed of light. These projectiles serve as a nearly instantaneous source of excitation along their trajectory. In this investigation, we use only thin targets and projectiles near their equilibrium charge-state. Thus, the ions lose only a minor part of their energy, and their charge-state is approximately conserved. We present and discuss total electron yields, as well as Auger- and convoy-electron spectra taken for 5 MeV/u heavy ions (N, Ne, S, Ni, and Ag) interacting with carbon foils (representative for conducting materials) and with polypropylene foils (representative for an insulator). In the next section, the experimental methods are described; then follows a section on theoretical considerations on the time-dependent electron density and ion-induced potentials in solids, and in the final section, the experimental data are presented and discussed in the light of theoretical estimates.

Experimental Methods

In the following, we give a brief description of the experimental setup. A more detailed description can be found in previous publications [96, 100]. Most results that are presented in this work have been obtained with heavy ions (with nuclear charges in the range from Z = 7 to 47) at an incident energy of 5 MeV/u. The beam was delivered by the heavy-ion cyclotron of the **I**onen**s**trahl-**L**abor (ISL) at the Hahn-Meitner-Institut, Berlin. Both the 5 MV Van-de-Graaff and the 8 MV tandem accelerator were used as injectors for the cyclotron. The beam was send through a post-cyclotron stripper foil to determine the mean equilibrium charge-state and to select magnetically a projectile charge-state close to equilibrium. The charge states determined in this way agree very well with the *ab initio* predictions of Rozet *et al*. [85, 86].

Before entering the magnetically shielded target chamber, the beam of typically 0.1 to 10 particle nA was collimated to about 1 mm^2. Up to 14 solid-state targets were mounted in the middle of the chamber on a rotatable disc that is connected to a target wobbler. Wobbling of the targets in both directions perpendicular to the beam is essential for accurate fluence determinations in the case of well focused beams. All data that are presented and discussed in this work correspond to normal incidence conditions. The ratio of the currents from the target and the Faraday cup allows a determination of the total yield of ejected electrons, since the mean projectile charge-state is known, and sputtering from the carbon surfaces is of minor importance compared to the large number of ejected electrons. Behind the target, a surface barrier detector was placed very close to the beam axis and allowed an energy determination of scattered projectiles after elastic or quasi-elastic interactions with carbon nuclei of the material.

For the key point of this investigation, the measurement of electron energy-spectra, two electrostatic electron spectrometers were used. For the determination of zero-degree electron spectra (ejection in beam direction) a tandem spectrometer was used [59, 60, 112], where the primary beam can pass through the first stage of the analyzer. The measurement of target Auger-electron energy distributions was performed with a single-stage parallel-plate spectrometer at an ejection angle of 135° [111]. The uncertainty of the energy calibrations is about ± 0.5 eV.

The experiments were performed with two types of target foils, namely amorphous carbon foils of 3, 20 and 100 μg/cm^2 and also with polypropylene (PP, $[C_3H_6]_n$) foils at thicknesses of 0.5 and 1.5 μm. An Auger-spectroscopic surface analysis showed that the PP samples have a 5% O contamination, and the carbon samples have a 3% O contamination near the surface that might stem from H_2O. These contaminations are expected to lead only to minor uncertainties for the present investigation. Two serious problems, however, exist for the PP foils: beam-induced melting and evaporation due to the low heat conductivity and also macroscopic charging due to the low electrical conductivity. We have solved both problems by evaporating a conducting film on one side of the sample. For the results presented in this work, we have used Al coatings of 20 and 30 μg/cm^2 and for the PP substrate we expect a maximum temperature rise of less then 50 K for the highest ion flux during the irradiation.

The effects of macroscopic charging are easy to observe for electron irradiation [31]. Within some minutes, the target-Auger lines, that we have measured for 3 keV electrons on PP, were shifted to higher energies by up to a few

hundred eV. When the shift was approaching a breakthrough voltage, it was suddenly reduced, and the charging-up process was repeated. By reducing the electron currents from about 10 nA (similar as in the ion experiments) down to 1 nA, the time scale of these fluctuations was extended as expected. In contrast to the electron measurements, we found no such indications for charging up in the case of heavy-ion irradiation at the same incident velocity. Here we found sharp Auger- and convoy-line structures, and no significant dependence of the target/beam current ratio on the beam current. This allows us to put an upper limit of about 3 V on fluctuations and about 20 V on the absolute value of a surface potential due to macroscopic charging in PP.

The low-energy electron spectra, however, indicate a shift of the continuous spectral structure toward lower energies in the case of low fluences. With increasing fluence, this shift vanishes, since the foils loose their hydrogen contents during irradiation, the so-called carbonization process. At the highest fluences investigated in this work, the relative hydrogen contents is reduced from 66% to below 50% [96, 100]. This leads to an increased conductivity and reduced recombination times, as can be seen from the Auger- and convoy-electron spectra, as well as from dc-resistivity measurements. It is emphasized that the electrons at energies below about 50 eV are mainly created via electron-electron collision cascades [99, 104] and penetrate the surface further away from the ion path (typically 20 to 100 Å). Thus, the electron spectrum close to zero energy will predominantly be influenced by macroscopic surface potentials and less efficient by any track effect.

Figure 1 displays low-energy part of the first (circles) and the last (squares) spectrum of a series of measurements taken for 5 MeV/u Ar^{16+} projectiles with the same 1.5 µm PP sample. The fluence differs by about two orders of magnitude between the two measurements. The low-energy part below about 20 eV shows a strong increase with increasing fluence (see the inset in Fig. 1) and the final spectrum is similar to the one for amorphous carbon (not shown in the figure). As will be shown in the following, this increasing intensity at low energies is a result of decreasing macroscopic charging and of a conductivity enhancement in the sample. If we assume that chemical changes of the sample do not influence the spectrum inside the solid and that the macroscopic field between sample and spectrometer may be approximated by a planar potential, we may transform the singly differential energy distribution dN/dE for a sample without macroscopic fields into a spectrum dN'/dE under the influence of a positive surface potential ΔV using

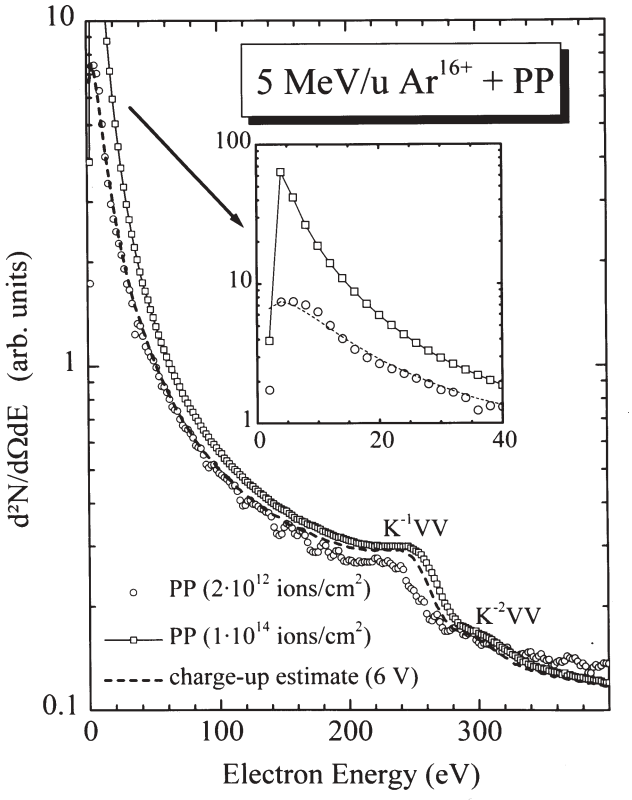

Figure 1. Experimental low-energy electron-spectra for 5 MeV/u Ar^{16+} ions on polypropylene (PP) measured under a backward angle of 135° at two different fluences. The carbon KVV-Auger structures for single and double K vacancies are also visible. The dashed line is explained in the text.

$$\frac{dN'}{dE}(E) = \frac{dN}{dE}(E + \Delta V) \cdot \frac{E}{(E + \delta E)} \qquad (1)$$

where E is the electron energy with respect to the vacuum level. The original spectrum is shifted by the potential ΔV, and the last term describes the refraction at a finite planar potential [81, 105, 106, 110; also, private communication with M. Rösler, 1993]. In our experiments, there are deviations from the planar symmetry that should increase the refraction effect. On the other hand, the carbonization and the corresponding compaction may lead to an enhancement of the microscopic sample-surface potential by about 2 eV at high fluences. For the determination of ΔV, both effects tend to cancel each other.

The dashed line in Figure 1 shows the result of eq. (1), where the experimental high-fluence data are transformed using ΔV = 6 V. Below an energy of about 100 eV, there is good agreement of this curve with the low-fluence spectrum.

The fit gives accurate results for ΔV, so that the main uncertainties for the charging are due to the approximations involved in eq. (1). At energies of about 250 and 300 eV, there are structures superimposed on the continuous spectrum in Figure 1. These structures are due to carbon KVV-Auger electrons from the target, and they are shifted by about 18 eV between both measurements. The dominant contribution to this shift is produced by the nuclear-track potential [96, 100], as will be discussed in **Results and Discussion**.

We have performed fits, using eq. (1), for several spectra due to N-, Ne- and Ar-ions. A macroscopic charging-up of 6 to 12 eV is consistent with all of our observations and determines also the uncertainty for the carbon KVV Auger results in the case of heavy ions interacting with 1.5 μm PP foils. For the 0.5 μm PP foils, the charging was reduced by approximately a factor 3, and for N ions, we found larger macroscopic charging effects than for the heavier ions. It is noted that a macroscopic charging of 30 to 40 V was observed for N ions penetrating polycarbonate samples. Thus, electron recombination is less effective in this material, and consequently, significant quantitative results on microscopic effects can hardly be obtained with polycarbonate samples.

The heavy ions produce ionization tracks that seem to enable recombination via the Al surface film. We found a rise in the conductivity of PP (measured between both sample surfaces) by several orders of magnitude and enhanced recombination rates (see **Results and Discussion**) after heavy-ion irradiation. For the light Li ions, no change of the conductivity was observed, and for N projectiles, there is an increased charging of the samples as compared to heavy projectiles. The maximum charging-up increases by orders of magnitude for incident electrons. Thus, the continuous ionization tracks produced by highly charged heavy ions appear to be responsible for the small macroscopic charging observed in PP.

Theoretical Considerations

Before details of ion-induced potentials in solids are discussed in this section, some more general remarks on electron densities of isolated atoms as well as solids may be in order. The time-dependent local electron density $\rho(\mathbf{r}, t)$ in a crystal that is perturbed by a heavy charged particle of nuclear charge Z_p moving along the trajectory $\mathbf{R}_p(t)$ reads (in atomic units)

$$\rho(r, R_p, t) = \sum_{\substack{n_0,\ \mathbf{k_0} \\ E_0 < E_F}} |\psi_{(n_0,k_0)}(t)^2 \qquad (2)$$

where n_0 is the initial-state band index at $t \to -\infty$, $\mathbf{k_0}$ is the Bloch wave vector and Ψ is the time-dependent wave-function evolving from each initial state. The sum extends over all initial states with energies E_0 below the Fermi energy E_F. For simplicity, we will not discuss antisymmetrization effects or the influence of correlation. Hence, we adopt the independent-electron model, replace n and k by a common index and write

$$\psi_{(0)}(r, R_p, t) = a_{0,0}(t) \cdot e^{-iE_0 \cdot t} \cdot e^{ik_0 \cdot r} \cdot \phi_0(r) + \sum_{\substack{j \\ E_j > E_F}} a_{j,0}(t) \cdot e^{-iE_j \cdot t} \cdot e^{ik_j \cdot r} \cdot \phi_j(r) \qquad (3)$$

The functions $e^{i\mathbf{kr}} \cdot \phi$ are the stationary Bloch wave-functions, and ϕ is periodic with respect to the crystal structure. ϕ may be obtained from modern band-structure calculations with a sufficiently high degree of accuracy. The time-dependent amplitudes $a_{j,0}$, however, have not been calculated rigorously for any system. It is noted that the modulus square of the initial state amplitude corresponds to the density of states of the unperturbed solid. If the density changes $\Delta\rho(\mathbf{r}, \mathbf{R_p}, t)$ in eq. (2) are small compared to the initial electron density $\rho_0(\mathbf{r})$ one may apply perturbation theory (first order Born approximation) to the determination of the amplitudes. This means that we replace $a_{0,0}$ by a certain constant value for each initial state and require that couplings between intermediate excited states are of minor importance. Hence, we may write

$$a_{j,0}(t) = -i \cdot a_{0,0} \int_{-\infty}^{t} dt' e^{i(E_j - E_0)t'} \langle \phi_j | e^{i(k_0 - k_j)r} \cdot V(r - R_p(t')) | \phi_0 \rangle \qquad (4)$$

where $V(\mathbf{r} - \mathbf{R_p})$ is the perturbing potential, i.e., the projectile Coulomb potential screened by bound projectile electrons and modified by the collective screening due to all other target electrons. To our knowledge, an equation equivalent to eq. (4) has been solved only for intraband transitions induced by protons at low velocities for channeling and random directions in Na and Li crystals [46, 94, 95]. The solutions of eq. (4), however, are proportional to an effective charge Z_{eff} that depends on the energy transfer during the excitation. At this point, we insert eq. (3) into eq. (2), using our knowledge that $a_{j,0} \approx Z_{eff}$ and get

$$\rho(r,R_p,t) = \rho_0(r) + Z_{eff}\cdot f_1(r,R_p,t) + Z_{eff}^{\,2}\cdot f_2(r,R_p,t) \quad (5)$$

where the function f_2 corresponds to products of excited-state wavefunctions ϕ_j and f_1 corresponds to the cross terms involving the initial-state wavefunction. In a treatment that goes beyond perturbation theory, all orders of Z_{eff} would come into play, and the contribution due to the initial-state density is reduced because of the transitions to all final states. From eqs. (3) and (5), we can see that the first two terms on the right hand side correspond to linear response theory [39, 46, 69, 80, 94, 95], if we replace the wavefunction ϕ_j by 1 (plane waves). The last term corresponds to products of excited-state amplitudes. This term gives only a small contribution to transient density changes **inside the solid**, since the excitation amplitudes are required to be small if perturbation theory is valid. **Outside the solid**, the first two terms approach zero because the initial-state density is bound to the solid, with an exponential decaying density outside the surface. Furthermore, the integral over the second (linear) term is zero ($\int d\mathbf{r} f_1(\mathbf{r}) = 0$). Thus, the last term describes electron ejection, if the energy dissipation in electron-electron interactions is neglected. This means, measured electron intensities or ionization cross sections are proportional to Z_{eff}^2, and density changes inside the solid are proportional to Z_{eff}, as long as perturbation theory holds. Deviations from such a behaviour, the so-called non-linear effects, will be shown and discussed in this work. It is noted, that the above discussion is valid for any solid, but from this point on, we will deal only with amorphous solids, respectively with non-channeling (random) motion of the projectile.

Echenique, Brandt and Ritchie [39, 80] have shown how to calculate the time-dependent electron density and the ion-induced potential, for different dielectric functions $\varepsilon(\mathbf{k},\omega)$ in the linear response theory. The results include single-particle excitations as well as collective excitations and are based on the homogeneous electron-gas picture of a solid. For highly charged projectiles, however, the linear response theory is expected to fail. Furthermore, the local variations of the solid-state potential due to the target nuclei, the corresponding localized states, energy dissipation via electron-electron interactions and electron tunneling are not incorporated in the model. Thus, one may expect a poor representation of the excitation and recombination processes in semiconductors and insulators; or, more rigorously, for all bound electrons below the conduction band. The induced wake potential Φ, at a radial distance r from the projectile path and for the coordinate z^* in the projectile frame of reference, is given for a

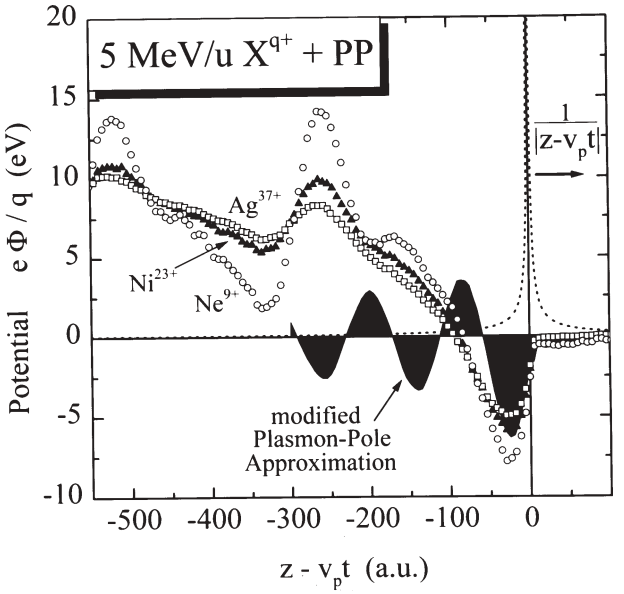

Figure 2. Non-perturbative theoretical results (CTMC results for Ne^{9+}, Ni^{23+} and Ag^{37+}) for the scaled track potential $e\cdot\Phi/q$ in polypropylene (PP) as function of the projectile charge-state q. The dotted curve shows the projectile Coulomb potential, and the arrow shows the flight direction. The shaded curve corresponds to the linear-response estimate for PP, using a generalized plasmon-pole dielectric function.

---

projectile of charge Z_p and velocity v_p by

$$\Phi(r,z^*) = \frac{Z_p}{\pi\cdot v_p}\int_0^\infty d\kappa \frac{\sin(r\cdot\kappa)}{r}\int_{-\infty}^{\infty} d\omega \frac{e^{i\omega\cdot z^*/v_p}}{[k^2\cdot\varepsilon(k,\omega)]} \quad (6a)$$

with $k^2 = \kappa^2 + \omega^2/v_p^2$. Accounting for the finite energy gaps ω_g, one may generalize the plasmon-pole dielectric function [39, 54, 80] to consider all valence- and inner-shell bands according to

$$\varepsilon(k,\omega) = 1 + 4\pi\rho_m \sum_n \frac{N(n)}{\omega_g^2(n) + \beta^2 k^2 + k^4/4 - \omega[\omega + i\gamma(n)]} \quad (6b)$$

where N is the occupation number for each band n (density of states). For the dielectric function of polypropylene ($[C_3H_6]_n$) we have used ω_g = 0.178, 0.481, 10.55 and 0.316 as energy gaps

of the three shells of carbon and the hydrogen 1s-shell. The molecular density is denoted ρ_m, $\beta = 0.78$ is related to the conductivity and $\gamma = 0.25$ is a damping constant that gives a rough estimate of the recombination behaviour and energy dissipation.

Figure 2 displays the scaled dynamic ion-induced potential $e \cdot \Phi/q$ (solid curve with shaded area) calculated with the dielectric function defined above for polypropylene. The projectile Coulomb potential is also displayed (short-dashed curve) and in linear response theory, both potentials are proportional to the projectile charge q. It is seen that the induced potential goes through a minimum with negative values directly behind the projectile position. This is a result of the enhanced electron density due to the attractive projectile potential. It is noted that the derivative of the induced potential at the projectile position ($r = z - v_p \cdot t = 0$) is directly proportional to the ion stopping power. Further away behind the projectile, the induced potential shows damped oscillations, the so-called wake potential. The reason for the oscillations in this model is a collective effect. Initially electrons pile up at the center of the ion path, and the repulsive electron-electron interaction induces an electronic motion away from the z-axis. This leads to a significant reduction of the electron density at a later time, the electronic motion will be reversed and so forth.

In an insulator, electron recombination can be suppressed due to traps (localized excitons and color centers) and low tunneling rates. Thus, we will describe a new model that is complementary to the above discussed electron-gas model and that should be more reliable for insulators. We will neglect collective effects and electron recombination in our treatment, but will account for energy dissipation of electrons as well as the target nuclear field. Furthermore, projectile-electron interactions beyond first order perturbation theory will be considered, and thus, there is no restriction on the projectile charge.

As we have discussed in detail in a previous work [46, 94, 95], high-energy excitations from any state of a solid as well as excitations of strongly localized states are better described in an atomic collision model than with an electron-gas model. Here we have performed CTMC (classical-trajectory Monte Carlo) calculations for different impact parameters b and for each individual target shell n [15, 93, 115]. A Monte Carlo integration technique is used to calculate the time-dependent evolution of the electron density under the influence of the electrostatic potential of a target core and the unscreened projectile Coulomb-potential. Test calculations for a restricted impact-parameter range indicated that the collective screening will lead only to minor deviations. The target field is given by a Coulomb potential, with an effective charge dependent on the shell under consideration, and the initial electron density is given by a microcanonical ensemble. The CTMC model, similar to all other classical models of electronic motion, does not account for long-range dipole interactions [15, 115] that will (at least partially) lead to plasmon creation in solids. For highly-charged particles, however, dipole interactions are suppressed [48]. It was shown that the CTMC method yields reliable results for heavy particles interacting with atoms, but fails for small perturbations of the target system as, e.g., for fast incident protons [48].

We have modified our CTMC code to account for electron-energy dissipation in the medium: electrons that move outside the Wigner-Seitz cell of their parent nucleus are decelerated according to a continuous slowing down model, so that the electrons stop at a certain distance from the parent nucleus. These calculations yield the densities of nuclei ρ^+ and electrons ρ^- as a function of time t, the radial distance r' from the track and the distance z' with respect to the projectile along the track. For non-interacting atoms of nuclear charge Z_A and atomic density ρ_A, distributed randomly in the solid, the averaged net-charge density reads (in a.u.)

$$\overline{\Delta\rho}(r',z') = 2\pi \cdot v_p \cdot \sum_A \rho_A \int_{-\infty}^{\infty} dt \cdot \int_0^{\infty} db\, b \cdot [Z_A \cdot \rho^+(r',z',t,b) - \sum_{n=1}^{Z_A} \rho_n^-(r',z',t,b)] \tag{7}$$

where the index A corresponds to carbon and hydrogen atoms, respectively. The time-dependent charge densities stem from an average over 10^4 classical electron trajectories for each target shell. These trajectories represent exact numerical solutions of the classical three-body problem. The induced bulk potential Φ, at a distance r from the center of the track, and for the coordinate z in the laboratory frame of reference is given by

$$\Phi(r,z^*) = -V_{surface} + 2\pi \cdot \int_{-\infty}^{\infty} dz' \int_{r_0}^{\infty} dr'\, r' \frac{\overline{\Delta\rho}(r',z')}{\sqrt{(r'-r)^2 + (z'-z^*)^2}} \tag{8}$$

with $z^* = z - v_p \cdot t$. The lower limit $r_0 = 0.6$ a.u. was chosen to exclude the charge-density contribution at the center of the track. This is necessary in order to avoid double counting of charges, since at a later point, we will include the action of localized atomic ionization at the center-of-track by using atomic Hartree-Fock energies for a given degree of ionization.

The surface potential $V_{surface}$ can be extracted from the target potential calculated without external field (q = 0). The surface potentials that have been derived from our independent-atom CTMC charge distributions are 9.3 eV for PP and 23.3 eV for graphite. A more accurate value for graphite is 24.9 eV, as obtained from solid-state band-structure calculations [70, 74].

Figure 2 displays our non-perturbative theoretical results for the scaled ion-induced potentials $e \cdot \Phi/q$ along the z-axis for different projectile charge-states q in PP. The curves denoted CTMC were calculated as described above and are subject to statistical uncertainties of about 2%. It is seen that the CTMC values for heavy ions are similar to the electron-gas results near the projectile nucleus. At larger distances behind the projectile, however, there are oscillations superimposed on a continuously rising potential that reaches an equilibrium at a value of about $q \cdot 10$ eV.

The potential minimum directly behind the projectile position is due to the attractive field of the ion. In contrast to the electron-gas results, the oscillations are not related to collective-field effects {no collective-field effects are accounted for in eqs. (7 and 8)}. Instead, they are due to charge-density fluctuations localized near the atomic nuclei and may be assigned to the atomic excitation spectrum. Thus, in the electron-gas picture oscillations result from the mean **electronic field**, and in our independent-atom CTMC model, oscillations are due to the interaction between bound electrons and the corresponding **target nuclei**.

The equilibration of the induced potential in PP at non-zero positive values corresponds to ionized electrons that stop further away from the track. This contribution to the induced potential far behind the projectile and its equilibrium value will be named nuclear-track potential in the following. The nuclear-track potential is proportional to q^2 for projectile charge-states $q << 7$ (not shown in the figure), and it is nearly proportional to q for heavier ions [96, 100]. According to the discussion of eqs. (2) to (5), a permanent density reduction proportional to q^2 at the center of the ion track would be a non-linear effect for non-localized electrons. For localized electrons, however, the function f_1 might be close to zero near the track, so that only a quadratic q-dependence is left. Hence, at least for $q >> 7$, the behaviour of our CTMC results far behind the projectile is related to a non-linear effect. This nuclear-track potential represents the main difference in comparison to metal targets and it can be measured, as will be shown in the following section. It should be stressed at this point that recombination in a metal is much faster (typically 10^{-16} s) than in insulators, and correspondingly a treatment as described above cannot be applied to collective-field effects in metals. For metals, one still has to rely on electron-gas models.

Results and Discussion

In the following subsections, we will deal with electron ejection from (semi-) conducting amorphous carbon samples and insulating polypropylene (PP) samples. One may sort the different target types according to their conductivity: metals, semi-metals and semi-conductors, insulators, frozen and atomic gas targets. With respect to electron dynamics, it is necessary to distinguish between excitation and transport processes.

As discussed in detail by Inokuti [56], only conduction/valence-band excitations may show significant differences between solids and gas targets. In another work it was shown [46, 94, 95], that even these differences disappear for high energy excitations of conduction-band electrons. Thus, only low-energy excitations of weakly bound electrons are sensitive to the solid-state structure. This includes single-electron excitations and, of course, collective excitations (plasmons).

Concerning the projectile screening there are significant differences between solids and gas targets. Fast projectiles approach increased charge-states due to the high collision frequency in solids, and correspondingly, there are increased excitation rates and stopping powers compared to gas targets, as known from many experimental and theoretical investigations. In a recent investigation, however, it was shown that the collective screening in a solid may also reduce the stopping power of intermediate- and low-energy ions [3, 6].

The transport of electrons in solids is determined by elastic and inelastic scattering processes [14, 53, 78, 81, 82, 84, 92; also, private communication with M. Rösler, 1993]. Elastic scattering gains importance with increasing target nuclear charge and inelastic scattering processes of fast electrons are determined mainly by the density of weakly bound target electrons. The transport of low-energy electrons, however, is very sensitive to the solid-state structure. In metals and semi-metals, the electron stopping power near the Fermi velocity is strongly reduced as a consequence of the Pauli exclusion principle [64]. Near the Fermi level electron-photon couplings and even crystal imperfections gain importance. Slowing down in other targets is strongly influenced by the gap ΔE_g between the valence and conduction band. For a review on electron slowing down in gaseous targets, the reader is referred to works by Inokuti and Kimura [57, 63]. With respect to electron ejection from solids, one may distinguish between two types of insulating materials depending on the electronic band gap and on the electron affinity A. Those materials for which $A < \Delta E_g$ holds true will lead to an increased low-energy electron ejection, since electrons below an energy of $\Delta E_g - A$ with respect to the vacuum level cannot loose energy via electronic excitations. This requirement is fulfilled by many

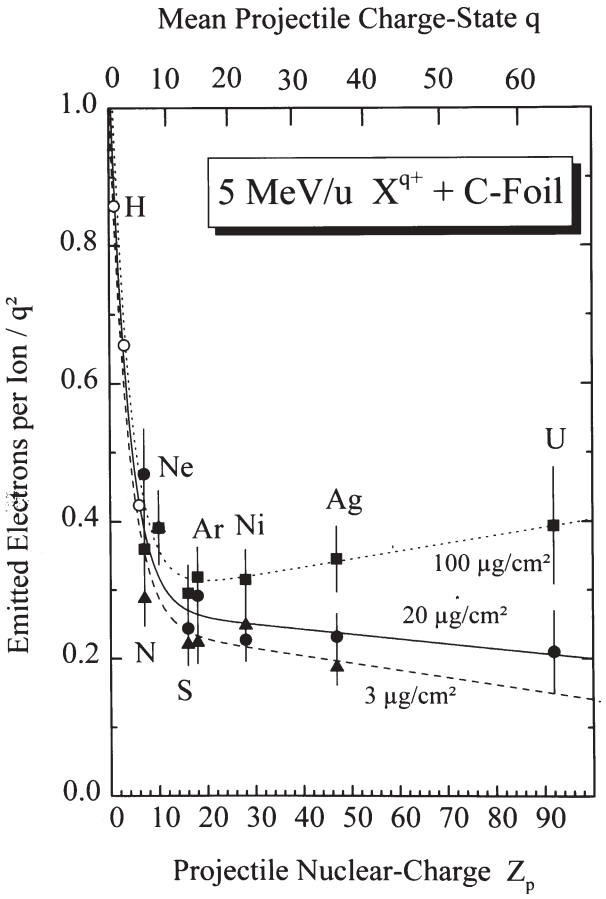

Figure 3. Scaled total electron emission yields γ_e/q^2 for 5 MeV/u heavy ions near the equilibrium charge state penetrating carbon foils under normal-incidence conditions. The investigated target thicknesses are 3 (triangles), 20 (circles) and 100 µg/cm² (squares). The data for $Z_p < 7$ (hollow circles without error bar) have been taken from refs. [33, 34].

large-band-gap materials (LiF, diamond, frozen rare gases).

Total electron yields

Electronic effects are often discussed in terms of the electronic stopping power S_e. This is true also for the total electron yield γ_e. Some approximate solutions of the transport equations predict a proportionality between both quantities [105, 106, 110]. From other electron-transport models, it emerges that such a proportionality is not self-evident and could be only due to cancellation effects [81, 99, 104; also, private communication with M. Rösler, 1993]. In fact, for light projectiles in different materials, a proportionality between S_e and γ_e, with varying material constants, was found for a variety of projectile velocities [33, 34, 65]. Significant deviations from an S_e proportionality (up to a factor of two) have been found for heavier ions in previous works: with increasing projectile nuclear-charge, there is a reduction of the ratio γ_e/S_e [7, 8, 19-21, 32-34, 65, 71, 83]. This deviation was proposed to be due to a hypothetical positively charged ionization-track in metals that decelerates all electrons and lowers the number of emitted electrons [19-21, 65]. In this work, we concentrate only on one projectile velocity (14.1 a.u.) and present data that enable an interpretation of the Z_p dependence of the total electron yields from C foils.

Figure 3 displays scaled electron emission yields for 5 MeV/u heavy ions incident on carbon foils with their equilibrium charge states. The results for the 8 MeV/u U^{68+} ions (the stopping power of U in C at 8 MeV/u is to within 1% equal to S_e at 5 MeV/u) and 5 MeV/u Ne^{9+} ions have been reevaluated from the raw data of refs. [99, 104]. The data for 5 MeV protons in 20 µg/cm² C-foils have been taken from refs. [33, 34], and the data for Li and C ions have been extrapolated from results of the same work (open circles). The data for Z_p = 7, 16, 18, 28 and 47 have been determined in this work. Experiments were performed for carbon foil-targets of 3 (solid triangles), 20 (solid circles) and 100 µg/cm² (solid squares). The scaling variable q denotes the mean projectile charge-state. Theoretical predictions for the charge-state evolution [85, 86] have been used to extract the mean charge state in the center of the foil. Thus, the results presented here differ slightly (typically by less than 15%) from preliminary published results [96, 100], where the incident charge state was used.

The scaled stopping power S_e/q^2 for carbon, as has been measured by other authors for different projectiles at 5 MeV/u [43, 45], yields a nearly constant value for $Z_p < 15$. For a few projectiles (N, Ne, S, Ni, Ag), we have also determined the stopping power in an auxiliary experiment and find quantitative agreement with these more accurate results. From Figure 3, it is clear that the scaled electron yield Δ_e/q^2 is not constant and, thus, not proportional to S_e/q_2. There is a decrease of the scaled experimental electron yield for $Z_p < 15$ (about a factor of 3), with a tendency to approach a constant value at large Z_p. It should be emphasized at this point that we do not agree with the common assignment [7, 8, 19-21, 65] that low-energy electrons should be suppressed by a hypothetical positively-charged ionization-track, being a cylindrical trap for electrons.

As discussed in section 3, we expect dominant repulsive fields ($\Phi < 0$) directly behind the projectile and not attractive ones [39, 40, 67, 80]. Fast electrons will be **accelerated** by the collective potential, and slow electrons are influenced by the rapidly oscillating field in the case of metals. Thus, the proposed deceleration of electrons, due to a positive net charge at the center of the track [19-21, 65], is inconsistent with the

electron-gas theory of metals [39, 40, 67, 80]. Since the oscillating fields are not included in the track model of Borovsky and Suszcynsky [19-21], it should not be valid for metals.

Furthermore, this model predicts the electron yield γ_e to be proportional to $q^2 - c \cdot q^4$ for small values of q, whereas the fits in Figure 3 (an exponential plus a linear term) indicate a $q^2 - c \cdot q^3$ relation, with a material dependent constant c. This is an indication for an effect from second order perturbation theory, similar to the Barkas effect for stopping powers, and it might be related to a suppression of plasmons and low-energy electrons during the primary excitation process. It is noted that recent experiments by Y. Yamazaki *et al*. (private communication, 1996) for 5 MeV/u μ^+ and μ^- bombardment of a 10 $\mu g/cm^2$ carbon foil might be in contradiction with our fit curves at small q. The μ^+ and μ^- coincidence data for single-electron ejection are identical to within 2%, but from Figure 3 one would expect significantly enhanced electron yields for μ^- projectiles.

The thickness and charge-state dependence of the data for $Z_p > 15$ has been discussed in detail previously [96, 100]. The observed differences are due to the ejection of fast electrons that can penetrate the whole foil. These electrons are favorably produced by strongly screened heavy ions, such as U^{68+}.

Auger-electron emission

The modification of solids by fast highly charged ions may be due to high ionization densities near the center of the track. In practice, one would like to get quantitative results concerning primary ionization probabilities. This enables estimation of the maximum local ionization density near the track. Furthermore, it is possible to extract from such data whether there is a continuous ionization track or not. The integral number of inner-shell vacancies produced near the track can be determined from X-ray- or Auger-spectra observed in backward directions. The number and energy of δ-electrons ejected in backward directions is lower than in the forward hemisphere. Thus, δ-electron-induced inner-shell ionization is less likely to occur [98] at the beam-entrance side of the foil, and thus, vacancies are produced directly by the ion and near the center of the track. Nearly 100% of all inner-shell vacancies of carbon atoms decay via the Auger-process. Correspondingly, we have analyzed the target-Auger spectra for different projectiles. The integral cross sections are determined mainly by large-impact-parameter collisions (as compared to the shell radius) and yield no information on the ionization probabilities in violent encounters. Ratios of double- to single-ionization cross sections, however, are sensitive to the ionization probabilities in central collisions as will be shown in the following.

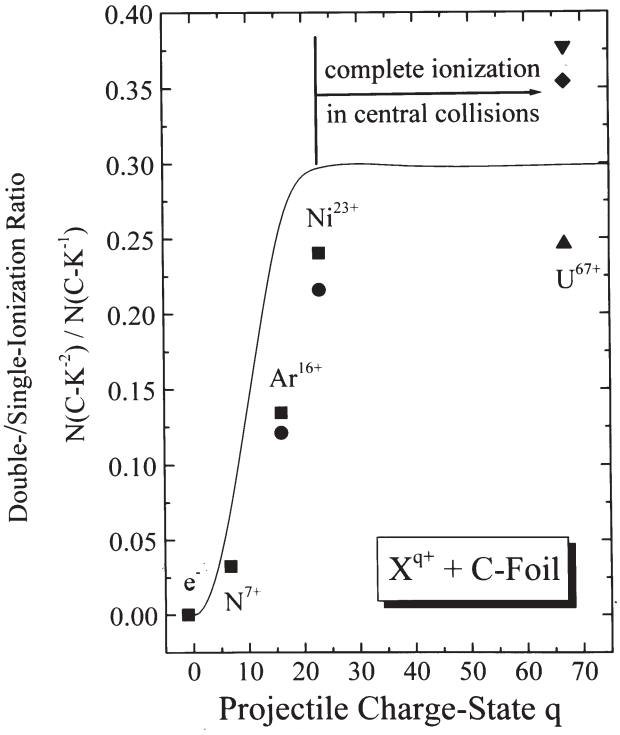

Figure 4. Ratio of double to single K-shell vacancies in carbon versus projectile charge state q. The solid line is obtained from the independent electron model and the Magnus approximation.

Figure 4 displays the ratio of double- to single-K-shell ionization cross sections in collisions of highly charged ions at 5 MeV/u with carbon atoms in an amorphous carbon environment. It is noted that similar results have been obtained from the carbon Auger-spectra of polypropylene targets (see Fig. 1). We have used two methods to determine the cross section ratios from the $K^{-1}VV$ Auger intensity at E = 253 eV and from the $K^{-2}VV$ intensity at an energy of E = 305 eV, yielding similar results:

$$\frac{\sigma^{2+}}{\sigma^{+}} \approx \frac{N_m(K^{-2}VV)}{N_m(K^{-1}VV)} \cdot \frac{S_e(E(K^{-2}VV))}{S_e(E(K^{-1}VV))} \approx \frac{N_i(K^{-2}VV)}{N_i(K^{-2}VV)} \cdot \frac{\lambda(E(K^{-1}VV))}{\lambda(E(K^{-2}VV))} \quad (9)$$

Here S_e is the electron stopping power at the energy E and λ is the corresponding electron escape depth. N_i is the yield determined from an integral over the Auger line and N_m is the

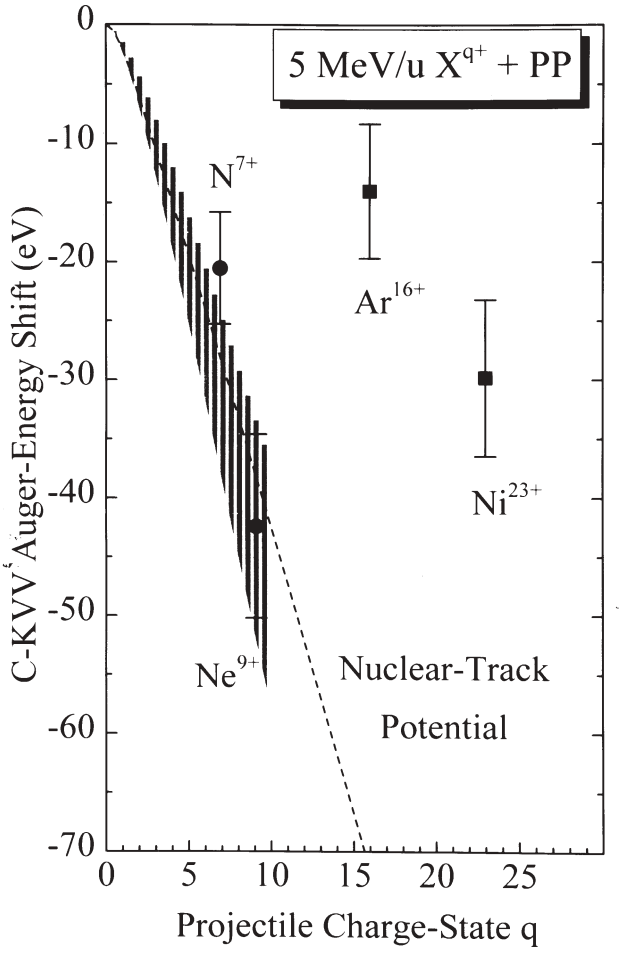

Figure 5. Experimental Auger-energy reduction and the corresponding prediction of the track model (shaded area) as a function of the projectile equilibrium-charge-state. Also shown is the bulk track-potential including quantum and collective-field correction (dotted curve).

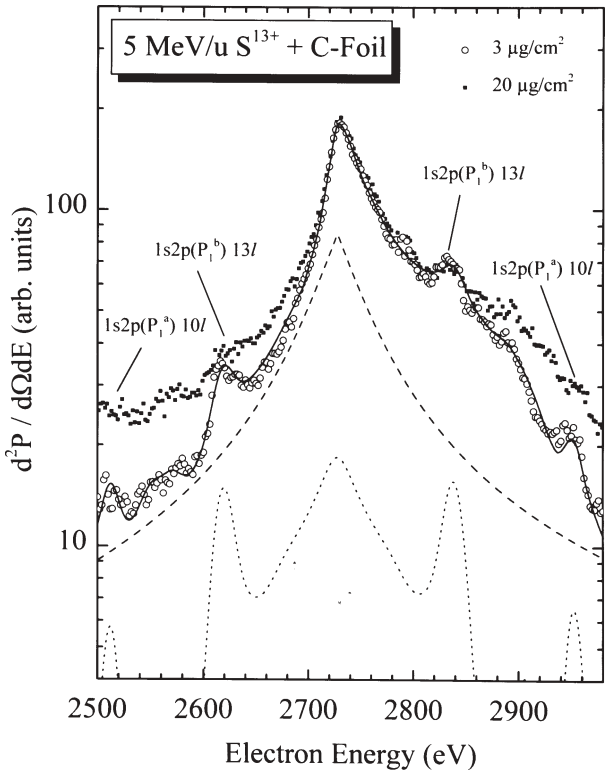

Figure 6. Convoy-electron spectra for 5 MeV/u S^{13+} + carbon foils at thicknesses of 3 (open circles) and 20 µg/cm^2 (solid squares). The dashed curve is the convoy-electron peak which is obtained from a kinematic transformation. The dotted curve shows the projectile Auger-peaks which are obtained from calculated Coster-Kronig transition energies. The solid curve shows the sum of both contributions, plus an estimate for the contribution due to field-ionized Rydberg electrons.

maximum line intensity, in both cases after background subtraction. Experiments have been performed for electrons, N, Ar and Ni in this work and previously also for U ions [99, 104] at about the same projectile velocity.

In an independent electron model (IEM) within first order perturbation theory, one expects σ^+ to be proportional to q^2 and σ^{2+} to q^4. Thus, the ratio should behave as q^2. This is not the case, as can be seen from Figure 4. Already the value for Ar projectiles is about 25% lower than expected from the scaled N result. Furthermore, for Ni and U ions, there is clearly a saturation of the cross section ratio. The solid line in the figure is a theoretical result, calculated within the Magnus approximation [87, 88, 119] for numerical wave-functions being eigenstates of a spherically averaged solid-state potential [48, 94, 95]. It is still based on the IEM, but goes beyond perturbation theory.

There is a qualitative agreement between the theoretical results and the data, the saturation values being the same. The ionization probabilities in the Magnus approximation are close to 100% at small impact parameters (corresponding to 250% in first order perturbation theory) for all shells in 5 MeV/u Ar^{16+} + C collisions and also heavier ions. Exactly these high ionization probabilities lead to the saturation observed in Figure 4. This clearly is a non-linear effect, and it is closely related to the fact that the nuclear-track potential scales quadratically with the projectile charge for light ions and only linear for heavy ions (CTMC in Fig. 2). The overestimated double-ionization cross sections for small q in Figure 4 are

known from investigations of ion-atom collisions. They are due to the neglect of dynamic screening and electron correlation in the double ionization process [111, 112]. Taking this failure of our model results into account, we estimate that there is **complete ionization of the K- as well as the L-shell** of carbon in central collisions with projectiles of charge-states $q > 24$ (indicated by an arrow in Fig. 4). For uranium ions, we expect a cylindrical volume with a diameter of 1 A around the ion path to be completely ionized.

In a previous work, we could show that there is a strong influence of the nuclear-track potential on the energy of emitted Auger electrons in 5 MeV/u Ne^{9+} interactions with PP and mylar foils [96, 100]. The positive net charge in the center of the track may survive long enough to decelerate Auger electrons, and corre-spondingly microscopic Auger-energy reductions of up 45 eV, with respect to carbon samples or carbonized PP samples, have been observed. Here we present measured Auger-energy shifts for N^{7+}, Ne^{9+}, Ar^{16+} and Ni^{23+} ions at 5 MeV/u as well as theoretical results from our CTMC model.

The bulk track-potential as derived from eqs. (7) and (8), at positions asymptotically far behind the projectile, has been corrected for collective effects (a reduction of the potential by up to a factor of 2 for $q >> 5$) and for quantum mechanical dipole contributions (an increase of the potential by up to a factor of 2 for $q << 3$) [96, 100]. It is emphasized that this determination of the nuclear-track potential (including non-perturbative and quantum effects) goes far beyond all track-potential models that are known to us [1, 19-21, 61, 79, 96, 100]. In most of these models, the impact-parameter dependence of ionization, quantum effects as well as non-perturbative three-body effects have been neglected. In the theoretical description of the track potential, as discussed so far, a certain region near the center of the track was excluded. This was done in order to include the effect of multiple ionization of the "Auger atom" in a more refined way. It leads to an Auger-energy shift that was estimated from theoretical outer-shell ionization probabilities [47, 91, 101] and from the corresponding atomic Auger-energy reductions of about 8 eV per outer-shell vacancy, obtained from the work by Schneider *et al*. [102].

Figure 5 displays our measured Auger-energy reductions together with the predictions of the above described track model as a function of the projectile equilibrium-charge-state. The Auger-energy shifts have been determined for such low fluences that the surface stoichiometry, extracted from the Auger intensities, is about equal to the bulk stoichiometry of unirradiated PP. All data have been obtained for Auger emission from the beam-entrance side of the sample, and correspondingly the Al layer was evaporated on the other side. These experimental data are corrected for macroscopic charging of the samples, contrary to the previously published values [96, 100]. The theoretical bulk track-potential is displayed as a dotted curve and includes the corrections for collective effects and dipole contributions, but not the enhancement due to the increased ionization density at the "Auger atom." The shaded area may directly be compared to the experimental Auger results. The lower limit is determined for Auger electrons from deep inside the bulk, and the upper limit of this area corresponds to the expected energy shifts for Auger emission from the surface (the value of the bulk potential is reduced by a factor of 2 at the surface).

The experimental data for light projectiles (N^{7+} and Ne^{9+}) are in good agreement with the theoretical expectation. For heavier projectiles (Ar^{16+} and Ni^{23+}), the shift is significantly lower than the bulk track-potential. For these ions, with $q > 10$, one cannot predict Auger-energy shifts in PP with a model that neglects electron recombination. For such high projectile charge-states, there are initially more than two outer-shell vacancies in the carbon atom; and an Auger decay is impossible with less than two outer-shell electrons. Hence, two electrons have to be recombined in order to allow an Auger decay. The Auger-energy shift for $q > 10$ is lower than the maximum shift in the shaded area. This might be an indication for a slow recombination that occurs sequentially, either from the outer part of track or along the track.

From the measured data, we can put limits on the recombination time in the track, since the Auger decay represents a clock. From the agreement between model results and experimental data for N and Ne, one may estimate that the recombination times in PP will exceed 15 fs (femtoseconds, 10^{-15}). Thus, the recombination in PP is slow compared to Auger decay times. A similar estimate of the recombination time is not possible with the data for $q > 10$, without any further information on the recombination behaviour. Also it is recalled that the Auger decay is impossible (the clock is stopped) as long as there are less than two outer-shell electrons near the carbon nucleus. If the recombination is very slow for $q > 10$, there is another process to fill the K vacancy, namely radiative decay. Such a decay, if it is important, would reduce the absolute Auger intensity. Furthermore, the ratio of $K^{-2}VV/K^{-1}VV$ Auger emission would be reduced by about a factor of 2. This ratio, however, is similar for PP and amorphous carbon, and the absolute Auger yield from PP compared to carbon is consistent with the different stoichiometry (to within an uncertainty of 20 to 30%). Hence, from theoretical radiative decay rates, we can put an upper limit of 10 ps (picoseconds, 10^{-12}) on the recombination time in polypropylene.

Convoy-electron energies

At an electron ejection angle of 0° with respect to the beam and for a velocity equal to the projectile speed, a cusp-

shaped peak appears in the spectrum of ejected electrons. For bare projectiles, the peak can be assigned to the so-called **E**lectron-**C**apture-to-the-**C**ontinuum (ECC) process [35, 68, 89], where a target electron is captured into a continuum state of the projectile. For projectiles carrying loosely bound electrons, a completely different process, namely the **E**lectron **L**oss into the projectile **C**ontinuum (ELC), leads to a similar peak structure [24, 113, 120]. Here projectile electrons are ionized at low energy transfers due to the interaction with screened target atoms. Both processes have been investigated intensively for gas targets [9, 22, 23, 69] and a similar peak, named convoy-electron peak, was also found for solid-state targets [51].

Figure 6 displays the convoy peak at an energy of about 2740 eV for 5 MeV/u S^{13+} ions penetrating carbon foils of 3 and 20 $\mu g/cm^2$. It is noted that the spectrum for the thicker foil has been shifted in energy, to allow for the projectile energy-loss in the foil. The convoy peak is dominated by the ELC [90], and it is also influenced by the ECC process, but collective effects [38] are unlikely to contribute significantly to the yield. Electrons that move with the projectile inside the solid are subject to a random walk under the influence of the attractive projectile potential as well as different interactions with the constituents of the medium [26, 28, 75]. In comparison to free electrons, convoy electrons travel for extended periods of time in the 0° direction [26, 28, 75, 97].

In general, the cusp peak is an effect of the attractive projectile Coulomb-potential of positively charged heavy particles. It may, however, also be viewed as a kinematic effect: if there is no significant post-collision interaction with the target and a non-vanishing energy distribution around zero kinetic energy in the projectile frame (this is also an indication for attractive potentials), the kinematic transformation of energy interval and solid angle from the projectile frame into the laboratory frame of reference will always lead to a pole exactly at the projectile velocity [36, 44]. Near its maximum, the shape of the measured peak is then only determined by the energy resolution and solid angle of the electron spectrometer. Such a simulated convoy peak is shown as dashed line in Figure 6 [121]. After its discovery, the convoy electron peak was assumed to coincide exactly with the projectile velocity. Only recently, it was found that convoy electrons may be **accelerated** due to the interaction with the projectile image-potential in glancing ion/metal-surface collisions [52, 76]. The first evidence for a convoy-electron acceleration under normal-incidence conditions has been presented recently for 5 MeV/u heavy ions interacting with carbon foils [121].

The experimental spectrum can be decomposed into three parts, which are convoy electrons (dashed curve), projectile-Auger electrons (dotted lines), and field-ionized Rydberg-electrons, respectively. The asymmetry of the experimental spectrum in comparison to the simulated convoy spectrum is ascribed to the contribution of Rydberg states ionized by the electrostatic field of the tandem spectrometer near the entrance slit of the first spectrometer stage [103]. The Rydberg spectrum enhances the intensity of the convoy spectrum on the high-energy side. Accordingly, a 1 eV energy shift of the experimental peak position may be induced.

The structures superimposed on both shoulders of the convoy-peak are recognized as the spectrum of projectile Auger states, which lead to 1s2pnl ($n > 9$) $\rightarrow$ 1s2sϵl' Coster-Kronig transitions. Each peak in the projectile frame appears twice in the laboratory frame, since the slow Coster-Kronig electrons are ejected in the forward and in the backward direction with respect to the fast moving projectile [59, 60, 112]. Under the assumption that the projectile velocity is equal to the convoy velocity, the peaks positions in Figure 6 have been determined from configuration-interaction Hartree-Fock energies [49].

A closer examination of Figure 6 shows that the theoretical prediction for the Coster-Kronig line positions is 7 eV too high in all cases. It is emphasized that the projectile Coster-Kronig-electrons are emitted, in case of the 3 $\mu g/cm^2$ foil, far behind the exit surface of the foil, since the penetration of the foil takes only a time of about 18 a.u., which is much shorter than typical Auger transition-times. This means that the Coster-Kronig lines are not influenced by any solid-state potential and allow a determination of the final projectile velocity [59, 60, 112]. Thus, we conclude that the convoy peak energy is 7 eV higher than the value expected from the final projectile velocity. This method of determining of the convoy energy shift relative to the projectile velocity is denoted **Auger method**. It has originally been applied by Yamazaki and Stolterfoht to the analysis of convoy-energy shifts, but no significant effect was found for two investigated ion-solid collision systems [122; also, private communication with Y. Yamazaki and N. Stolterfoht]. Another method of determining the convoy-energy shift is the **solid/gas method**. Here the convoy peak position is measured for a gas target (no surface potentials) as well as for foils of different thicknesses [121]. Extrapolation to zero foil thickness directly enables a comparison with the gas results, showing the influence of solid-state potentials on the convoy energy (results obtained with both methods are plotted in Fig. 8, which is discussed later).

Figure 7 shows the peak energy of convoy electrons for 5 MeV/u Ni^{23+} ions penetrating PP foils with the evaporated Al layer in beam direction (squares) and opposite to the beam direction (circles). Two different samples have been used for each of the two geometries, and the accuracy of the energy

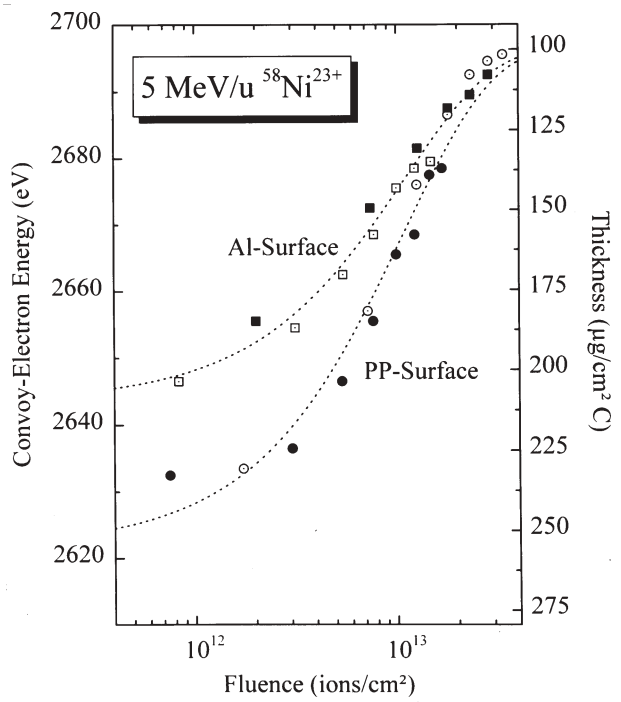

Figure 7. Peak energy of convoy electrons for 5 MeV/u Ni^{23+} + PP foils versus fluence. The upper data set (squares) was taken for the Al film, and the lower data set (circles) for the PP surface toward the 0° spectrometer. The dotted lines are fits to the data.

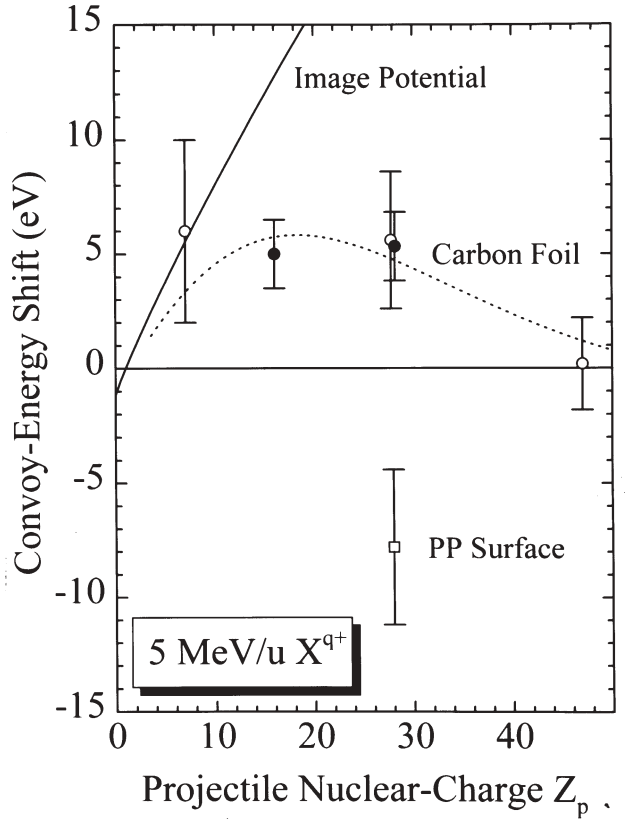

Figure 8. Energy shift of convoy-electrons for 5 MeV/u ions with respect to the projectile speed versus the projectile atomic number. The open circles are obtained with the solid/gas method and the closed circles are obtained from the Auger method. The solid line represents the estimated dynamic image potential using the model of refs. [25, 39, 80], and the dotted line is a fit to the data. The convoy-energy shift for PP (open square) is obtained from Figure 7 via the surface/surface method.

determinations is about 2 eV. It is seen that the energy of the convoy peak increases with increasing fluence. For the upper curve, our measured convoy-energy changes are consistent with the projectile-energy results obtained with a surface-barrier detector and also with the interpolated energy losses from refs. [13, 43, 123]. Carbonization of the PP foil leads to a reduction of the foil thickness, and correspondingly, to a reduced projectile energy-loss. This gives rise to an increased final projectile energy.

The lower curve, however, is influenced by additional solid-state potentials that vanish in the limit of high fluences. This behaviour is determined by the electron-recombination properties of PP, which change drastically with fluence, again as a result of carbonization. As discussed in **Experimental Methods** there is a macroscopic charging-up at the PP surface of about +9 V. Such a macroscopic charging can only explain 40% of the observed deviations between the Al and the PP measurements. Thus, the measured shift is, to a large extend, also of microscopic nature and reflects a single-track phenomenon. The absolute microscopic energy shift for PP may be deduced from the known macroscopic charging ΔV_{mac} and the microscopic shift $\Delta E(T)$ for a conducting target T as

$$\Delta E(PP) = \Delta E(Al) + \Delta E_{meas} - \Delta V_{mac} \qquad (10)$$

where ΔE_{meas} is the measured energy difference between PP and Al surface, as it can be obtained from Figure 7. For Ni^{23+} ions an auxiliary comparison of convoy electrons from thin C and Al targets has shown that $\Delta E(Al) \approx \Delta E(C)$, to within 0.5 eV. Thus, we replace $\Delta E(Al)$ by the known values of $\Delta E(C)$. This method of determining absolute microscopic energy shifts for thick foils will be named **surface/surface method**, since it is based on a comparison of the two surfaces of a sample.

Figure 8 displays the cusp-energy shifts, relative to the energy of electrons with projectile velocity, as a function

of the projectile atomic number Z_p. For most projectile ions, we have used the solid/gas method (open circles), and in those cases where significant Coster-Kronig lines are observable, we have applied the Auger method (closed circles). For Ni^{23+} ions, both methods were used, and the results are consistent with each other. It is seen that there is an **acceleration** of convoy electrons for the amorphous carbon target. This acceleration decreases significantly for heavier ions. The solid line is the dynamic image potential induced by the ion as well as by the convoy electron [25, 39, 80]. Its value is proportional to $\overline{q}$ -1, where $\overline{q}$ is the mean projectile charge-state after the passage of the foil. Contrary to the results for carbon foils, the measured microscopic energy shift for PP (open square), determined with the surface/surface method at low fluences, corresponds to a **deceleration** of convoy electrons.

Previously, we performed a preliminary surface/surface analysis of results for polycarbonate (PC) foils too, where a convoy deceleration of 35 ± 7 eV was measured for Ni^{23+} ions, and the macroscopic charging was assumed to be small compared to this value [121]. Using eq. (1) to determine V_{mac}, however, we find a charging of nearly 30 eV for PC in comparison to 9 eV for PP. Since the uncertainties add up to ± 12 eV for PC, it is not possible to give reliable results for polycarbonate foils.

Burgdörfer and coworkers have shown that the main features of convoy electron production and transport can be incorporated in a classical transport model [26-28, 75; also, private communication with J. Burgdörfer, 1995]. However, the corresponding Monte Carlo calculations are very time-consuming and, hence, it is not feasible to perform such calculations for our collision systems with low convoy-electron yields [27; private communication with J. Burgdörfer, 1995]. In a previous work, we have performed simplified Monte Carlo calculations for the penetration of a projectile-centered charge cloud, represented by a statistical electron ensemble, through a surface step-potential [121]. We have used a sudden approximation to describe the influence of the rapid passage through the surface-potential step on the electrons, and the final electron-momentum distribution incorporates the interaction with the highly charged projectile behind the surface. With realistic values for the potential (taken from refs. [25, 39, 80]) and for the radial extension of the convoy-electron distribution, we have computed a cusp shape similar as depicted in Figure 6, but without any significant energy shift. Only for potentials exceeding a few hundred eV or for radial extensions exceeding 50 a.u. at the surface, we found significant changes of the peak structure and also a shift of the cusp position. Hence, short-range potentials, as applied here, do not have a significant influence on the convoy-electron energy for the investigated cases.

Thus, we conclude that the long-ranging image potential of carbon is responsible for the convoy acceleration displayed in Figure 8. The reduction of this acceleration with increasing projectile charge is an indication for the competition between projectile charge and induced image charge. A qualitatively similar argument is: the formation of the cusp structure appears further away from the surface for heavier ions and, hence, the influence of surface potentials is reduced. It is emphasized that also non-linear effects might come into play. The finite electron density at the surface as well as the electron-electron repulsion can lead to a saturation of the image potential. A reduction of the potential with increasing projectile charge, however, seems to be not conceivable.

For the polypropylene target, the nuclear-track potential induced by highly-charged projectiles is likely to be the reason for the observed shift. This potential is expected to be about +100 eV inside the bulk for 5 MeV/u Ni^{23+} projectiles (see Fig. 5). The resulting convoy-electron deceleration at the PP surface is only 8 eV, as can be seen from Figure 8. We have found significant convoy-electron energy-shifts also for other projectiles, and the corresponding experimental results will be evaluated and published soon.

Conclusions

We have measured the total yield of ejected electrons, and we have investigated convoy, as well as C-KLL Auger, electrons for different heavy ions penetrating foil targets at 5 MeV/u. For the total yield of electrons ejected from carbon foils, we found clear deviations from the assumption of a proportionality with respect to the electronic stopping power of the projectile ions. It is noted that there are a few investigations in which such deviations from the assumed proportionality have been assigned to a hypothetical positively charged center of the track in metals [7, 8, 19-21, 65]. Such an assignment, however, is in contradiction with the electron-gas theory. Furthermore, our non-perturbative independent-atom calculations show that there is a negative net charge directly behind the projectile, even for an insulator. Thus, we expect the behaviour of the electron yields for Z_p < 15 to reflect a suppression of the ion-induced production of plasmons or low-energy electrons in the primary excitation process.

We have performed a systematic experimental and theoretical study of the C-KLL-Auger-energy shift induced by the transient **nuclear-track potential** in PP targets. We have presented an ionization-track model that includes a non-perturbative description of the electronic motion, collective-field as well as quantum corrections, and we find very good

agreement with our experimental data. From the uncertainty of the measured shifts for N and Ne projectiles, we could estimate that the recombination time in PP will exceed 1.5 x 10^{-14} s. From the measured C-KLL Auger intensities, for PP and C foils in the case of Ar^{16+} and Ni^{23+} ions, we conclude that fluorescence plays no significant role. Therefore, the recombination time will be below 10^{-11} s.

Additional Auger-peak determinations for incident electrons and heavy ions on carbon foils have been performed. These measurements indicate that the electronic recombination time is below 1 fs for this material, since we found no Auger-energy shift to within the experimental uncertainty of ± 0.5 eV. This is consistent with a recombination time of 0.1 fs, as estimated for an electron gas.

These Auger results do have some consequences for ion-induced material modifications:

(**1**) Our results for carbon foils show that there is a fast recombination. From the calculated time-dependent potentials, we expect a restricted Coulomb **implosion** and not an **explosion** [66] to occur in metals. At 5 MeV/u, the corresponding energy transfer will be less than 0.2 eV per atom even for U projectiles.

(**2**) High inner-shell ionization probabilities and even double-K-shell vacancies have been found in this work. Correspondingly, long-lived inner-shell vacancies (10^{-14} s) and the corresponding antibinding states may have some influence on modifications in PP as well as in amorphous carbon. The corresponding energy transfer may exceed 5 eV per atom in a narrow cylinder around the path of highly charged projectiles.

(**3**) For the polypropylene target, we find a recombination time between 15 fs and 10 ps. Thus, for heavy projectiles, Coulomb explosion will be important in this insulator, and the maximum energy transfer to the atoms near to the track can by far exceed energies of 50 eV (protons might even be accelerated by nearly the full track potential). At the surface, the nuclear-track potential is reduced by a factor 2 compared to the bulk value, since the atomic density corresponds to 50% of the bulk density. Furthermore, for slower projectiles (<< 5 MeV/u), we expect less effective charge separa-tions in the track and reduced track potentials. Thus, we estimate the energy of the fastest protons, desorbed due to Coulomb explosion, to be roughly 30 eV, in agreement with recent experiments for the interaction of fission products with different organic compounds [118]. Convoy-electron spectra for 5 MeV/u highly-charged ions penetrating carbon and polypropylene foils under normal incidence have been investigated experimentally. In the case of carbon foils, we have observed convoy-electron accelerations between 0 and 6 eV with respect to the projectile speed. Two different experimental methods have been applied for the determination of the projectile velocity and both give consistent results. The measured shift for carbon targets is most likely due to the long-range part of the dynamic surface-wake potential (image potential).

Contrary, for polypropylene foils we find decelerated convoy electrons (8 ± 3.5 eV for 5 MeV/u Ni^{23+} projectiles). This energy decrease seems to be related to the dynamic track potential that is formed during the electron/hole-pair creation near the surface. At present, it is not clear whether the observed energy shift for carbon as well as for polypropylene can be disentangled into separate contributions from the solid-state potential and from the projectile potential, or whether the polarization due to the simultaneous action of both fields cannot be separated.

Acknowledgements

We are indebted to N. Stolterfoht, A. Arnau and J. Burgdörfer for fruitful discussions. Furthermore, we would like to express our gratitude to the HMI-ISL accelerator crew for their excellent operation. This work was made possible via a DAAD scholarship of one of the authors (G.X.). Also we would like to thank J.P. Rozet for sending us the new version of his program "ETACHA" to calculate charge-state distributions.

References

[1] Akkermann A, Levinson J, Ilberg D, Lifshitz Y (1992) Track effects and their influence on heavy ion energy losses in semiconductor devices. In: Ionization of Solids by Heavy Particles. NATO Advanced Study Institutes Series 306. Baragiola R (ed.). Plenum Press, New York. pp. 431-438.

[2] Arnau A, Penalba M, Echenique PM, Flores F, Ritchie RH (1990) Stopping power for helium in aluminum. Phys. Rev. Lett. **65**, 1024-1027.

[3] Arnau A, Bauer P, Kastner F, Salin A, Ponce VH, Fainstein PD, Echenique PM (1994) Phase effect in the energy loss of hydrogen projectiles in zinc targets. Phys. Rev. **B49**, 6470-6480.

[4] Baragiola RA, Ziem P, Stolterfoht N (1976) Auger decay of excited Ar projectiles emerging from carbon foils. J. Phys. **B9**, L447-L451.

[5] Bates DR, Griffing G (1953) Inelastic collisions between heavy particles. I: Excitation and ionization of hydrogen atoms in fast encounters with protons and with other hydrogen atoms. Proc. Phys. Soc **A66**, 961-971.

[6] Bauer P, Kastner F, Arnau A, Salin A, Fainstein PD, Ponce VH, Echenique PM (1992) Phase effect in the energy loss of H projectiles in Zn targets: Experimental evidence and

theoretical explanation. Phys. Rev. Lett. **69**, 1137-1139.

[7] Benka O, Steinbauer E, Bauer P (1994) Kinetic electron emission yield induced by H^+ and He^{2+} ions versus stopping power for Al, Cu, Ag and Au. Nucl. Instr. Meth. **B90**, 64-66.

[8] Benka O, Schinner A, Fink T, Pfaffenlehner M (1995) Electron-emission yield of Al, Cu and Au for the impact of swift bare light ions. Phys. Rev. **A52**, 3959-3965.

[9] Berry SD, Sellin IA, Groeneveld KO, Hofmann D, Andersen LH, Breinig M, Elston SB, Schauer MM, Stolterfoht N, Schmidt-Böcking H, Nolte G, Schiwietz G (1983) Electron capture to the continuum at asymptotically high velocities. IEEE Trans. Nucl. Sci. **NS-30**, 902-905.

[10] Bethe HA (1930) Zur Theorie des Durchgangs schneller Korpuskularstrahlen durch Materie. Ann. Phys. **5**, 325-400.

[11] Betz HD (1972) Charge states and charge-changing cross sections of fast heavy ions penetrating through gaseous and solid media. Rev. Mod. Phys. **44**, 465-539.

[12] Betz HD, Grodzins L (1970) Charge states and excitation of fast heavy ions passing through solids: A new model for the density effect. Phys. Rev. Lett. **25**, 211-214.

[13] Biersack JP (1987) Three-dimensional distributions of ion range and damage including recoil transport. Nucl. Instr. Meth. **B19**, 32-39.

[14] Birkhoff RD (1958) The passage of fast electrons through matter. In: Handbuch der Physik. Vol. 34. Flügge S (ed.). Springer Verlag, Berlin, Germany. 53-138.

[15] Boesten LGJ, Bonsen TFM, Banks D (1975) Generalized oscillator strengths for the ionization of helium by protons, calculated with the classical three-body collision theory. J. Phys. **B8**, 628-637.

[16] Bohr N (1913) On the decrease of velocity of swiftly moving electrified particles in passing through matter. Philos. Mag. **25**, 10-31.

[17] Bohr N (1948) The penetration of atomic particles through matter. Dan. Mat.-Fys. Medd. **18**, No. 8.

[18] Bohr N, Lindhard J (1954) Electrons capture and loss by heavy ions penetrating through matter. Dan. Mat. Fys. Medd. **28**, No. 7.

[19] Borovsky JE, Barraclough BL (1989) High-velocity ionic projectiles interacting with metals: Models and measurements of secondary-electron yields from gold and aluminum targets struck by 13.5-31.5 MeV ^{7}Li and 9-63 MeV ^{12}C. Nucl. Instr. Meth. **B36**, 377-394.

[20] Borovsky JE, Suszcynsky DM (1991a) Experimental investigation of the z^2 scaling law of fast-ion-produced secondary-electron emission. Phys. Rev. **A43**, 1416-1432.

[21] Borovsky JE, Suszcynsky DM (1991b) Reduction of secondary-electron yields by collective electric fields within metals. Phys. Rev. **A43**, 1433-1440.

[22] Breinig M, Elston S, Sellin I, Liljeby L, Thoe R, Vane C, Gould H, Marrus R, Laubert R (1980) Initial tests of possible second-born-term source of asymmetry in forward electron ejection by fast bare nuclei. Phys. Rev. Lett. **45**, 1689-1692.

[23] Breinig M, Elston SB, Huldt S, Liljeby L, Vane CR, Berry SD, Glass GA, Schauer M, Sellin IA, Alton GD, Datz S, Overbury S, Laubert R, Suter M (1982) Experiments concerning electron capture and loss to the continuum and convoy electron production by highly ionized projectiles in the 0.7-8.5 MeV/u range transversing the rare gases, polycrystalline solids, and axial channels in gold. Phys. Rev. **A25**, 3015-3048.

[24] Burch D, Wieman H, Ingalls WB (1973) Electron loss in high-energy oxygen-ion collisions. Phys. Rev. Lett. **30**, 823-826.

[25] Burgdörfer J (1987a) Dynamical image charge effects on convoy electron emission from solid surfaces. Nucl. Instr. Meth. **B24/25**, 139-142.

[26] Burgdörfer J (1987b) Transport theory for convoy electrons and Rydberg electrons in solids. In: Lecture Notes in Physics. Vol. 294. Berenyi D (ed.). Springer Verlag. pp. 344-361.

[27] Burgdörfer J, Bottcher C (1988) Production of high-angular-momentum Rydberg states by stochastic collisions. Phys. Rev. Lett. **61**, 2917-2920.

[28] Burgdörfer J, Gibbons J (1990) Electron transport in the presence of a Coulomb field. Phys. Rev. **A42**, 1206-1221.

[29] Burgdörfer J, Meyer FW (1993) Image acceleration of multiply charged ions by metallic surfaces. Phys. Rev. **A47**, R20-R22.

[30] Burgdörfer J, Lerner P, Meyer FW (1991) Above-surface neutralization of highly charged ions: The classical over-the-barrier model. Phys. Rev. **A44**, 5674-5685.

[31] Cazaux J (1993) Some physical descriptions of the charging effects in insulators under irradiation. In: Ionization of Solids by Heavy Particles. Baragiola R (ed.). NATO Advanced Study Institutes Series 306. Plenum Press. pp. 325-50.

[32] Clerk HG, Gehrhardt HJ, Richter L, Schmid KH (1973) Heavy-ion induced secondary electron emission: A possible method for z-identification. Nucl. Instr. Meth. **113**, 325-331.

[33] Clouvas A, Rothard H, Burkhard M, Kroneberger K, Biedermann C, Kemmler J, Groeneveld KO, Kirsch P, Misaelides P, Katsanos A (1989) Secondary electron emission from thin foils under fast-ion bombardment. Phys. Rev. **B39**, 6316-6320.

[34] Clouvas A, Katsanos A, Farizon-Mazuy B, Farizon M, Gaillard MJ, Ouaskit S (1993) Projectile dependence of ion-

induced electron emission from thin carbon foils. Phys. Rev. **B48**, 6832-6838.

[35] Crooks GB, Rudd ME (1970) Experimental evidence for the mechanism of charge transfer into continuum states. Phys. Rev. Lett. **25**, 1599-1601.

[36] Dahl P, Rdbro M, Fastrup B, Rudd ME (1976) Auger spectroscopy on heavy-ion-atom collisions I. Kinematic effects and apparatus. J. Phys. **B9**, 1567-1579.

[37] Dalgarno A, Griffing GW (1955) Energy loss of protons passing through hydrogen. Proc. Roy. Soc. **A232**, 423-434.

[38] Day MH (1980) Wake-bound-electron contribution to convoy-electron velocity distributions: The effect of the ionic field. Phys. Rev. Lett. **44**, 752-756.

[39] Echenique PM, Ritchie RH, Brandt W (1979) Spatial excitation patterns induced by swift ions in condensed matter. Phys. Rev. **B20**, 2567-2580.

[40] Esbensen H, Sigmund P (1990) Barkas effect in a dense medium: Stopping power and wake field. Ann. Phys. **201**, 152-192.

[41] Fainstein PD, Ponce VH, Martinez AE (1993) Distorted-wave calculation of stopping powers for light ions traversing H targets. Phys. Rev. **A47**, 3055-3061.

[42] Fleischer RL, Price PB, Walker RM (1975) Nuclear Tracks in Solids. University of California Press, Berkeley, CA.

[43] Geissel H (1982) Untersuchungen zur Abbremsung von Schwerionen in Materie im Energie-bereich von (0,5-10) MeV/u, GSI-report 82-12. Darmstadt, Germany.

[44] Gordeev YS, Ogutsov GN (1971) On the interpretation of the energy spectra of electrons produced in atomic collisions. Zh. Eksp. Teor. Fiz. **60**, 2051-2059 (Sov. Phys. -JETP **33**, 1105-1109).

[45] Gorodetzky S, Chevallier A, Pape A, Sens JC, Bergdolt AM, Bres M, Armbruster R (1966) Mesure des pouvoirs d'arrêt de C, Ca, Au et CaF_2 (Calculation of the stopping powers of C, Ca, Au and CaF_2). Nucl. Phys. **A91**, 133-144.

[46] Grande PL, Schiwietz G (1992) Energy loss of slow ions: One-band calculation for alkaline metals. Phys. Lett. **A163**, 439-446.

[47] Grande PL, Schiwietz G (1993) Nonperturbative stopping-power calculation for bare and neutral hydrogen incident on He. Phys. Rev. **A47**, 1119-1122.

[48] Grande PL, Schiwietz G (1995) On classical calculations of the electronic stopping power at intermediate energies. J. Phys. B: At. Mol. Opt. Phys. **28**, 425-433.

[49] Grant IP, McKenzie BJ, Norrington PH, Mayers DF, Pyper NC (1980) An atomic multiconfigurational Dirac-Fock package. Comput. Phys. Commun. **21**, 207-231.

[50] Grove WR (1853) On some anomalous cases of electrical decomposition. Philos. Mag. **5**, 203-209.

[51] Harrison KG, Lucas MW (1970) Secondary electron energy spectra from foils under light-ion bombardment. Phys. Lett. **A33**, 142.

[52] Hasegawa M, Kimura K, Mannami M (1988) Convoy electrons emitted at glancing angle incidence of MeV light ions on the clean (001) surface of SnTe crystals. J. Phys. Soc. Jpn. **57**, 1834-1841.

[53] Hasselkamp D (1991) Kinetic electron emission from solid surfaces under ion bombardment. In: Particle Induced Electron Emission II. Springer Tracts of Modern Physics. Vol. 123. Springer Verlag. pp. 1-95.

[54] Inkson JC (1972) Many-body effects at metal-semiconductor junctions: I. Surface plasmons and the electron-electron screened interaction. J. Phys. **C5**, 2599-2610.

[55] Inokuti M (1971) Inelastic collisions of fast charged particles with atoms and molecules - the Bethe theory revisited. Rev. Mod. Phys. **43**, 297-347.

[56] Inokuti M (1991a) How is radiation energy absorption different between the condensed phase and the gas phase? Radiat. Eff. Defects Solids **117**, 143-162.

[57] Inokuti M (1991b) Subexcitation electrons: An appraisal of our understanding. Appl. Radiat. Isot. **42**, 979-983.

[58] Inokuti M, Dehmer JL, Baer T, Hanson JD (1981) Oscillator-strength moments, stopping powers, and total inelastic-scattering cross sections of all atoms through strontium. Phys. Rev. **A23**, 95-109.

[59] Itoh A, Schneider T, Schiwietz G, Roller Z, Platten H, Nolte G, Schneider D, Stolterfoht N (1983) Selective production of Auger electrons from fast projectile ions studied by zero-degree Auger spectroscopy. J. Phys. **B16**, 3965-3971.

[60] Itoh A, Schneider D, Schneider T, Zouros TJM, Nolte G, Schiwietz G, Zeitz W, Stolterfoht N (1985) Selective production of Li-, Be-, and B-like K vacancy states in fast Ne projectiles studied by zero-degree Auger spectroscopy. Phys. Rev. **A31**, 684-691.

[61] Jacobsson H, Holmen G (1994) Electron emission from ion-bombarded SiO_2 thin films. Phys. Rev. **B49**, 1789-1795.

[62] Johnson RE, Brown WL (1982) Electronic mechanisms for sputtering of condensed-gas solids by energetic ions. Nucl. Instr. Meth. **B198**, 103-118.

[63] Kimura M, Inokuti M, Dillon MA (1993) Electron degradation in molecular substances. In: Advances in Chemical Physics. Vol. 84. Prigogine I, Rice SA (eds.). John Wiley & Sons, New York. pp. 193-291.

[64] Kittel C (1986) Introduction to Solid State Physics. John Wiley & Sons, New York.

[65] Koyama A, Shikata T, Sakairi H, Yagi E (1982)

Dependence of secondary electron emission coefficients on z_1 in metal targets under bombardment with bare projectiles. Jpn. J. Appl. Phys. **21**, 1216-1221.

[66] Leseur D, Dunlop A (1993) Damage creation via electronic excitations in metallic targets. Part II: A theoretical model. Rad. Eff. Def. Solids **126**, 163-172.

[67] Lindhard J (1954) On the properties of a gas of charged particles. Dan. Mat. Fys. Medd. **28/8**, 1-57.

[68] Macek J (1970) Theory of the forward peak in the angular distribution of electrons ejected by fast protons. Phys. Rev. **A1**, 235-241.

[69] Meckbach W, Focke PJ, Goñi AR, Suárez S, Macek J, Menendez MG (1986) Effects of the Wannier ridge on secondary-electron spectra in proton-helium collisions. Phys. Rev. Lett. **57**, 1587-1590.

[70] Moruzzi VL, Janak JF, Williams AR (1978) Calculated Electronic Properties of Metals. Pergamon Press, New York.

[71] Oda O, Lyman JT (1967) Position and secondary-electron distribution for heavy ions. Rad. Res. Suppl. **7**, 20-32.

[72] Oen O, Robinson M (1976) Computer studies of the reflection of light ions from solids. Nucl. Instr. Meth. **132**, 647-653.

[73] Olivera GH, Martinez AE, Rivarola RD, Fainstein PD (1994) Electron-capture contribution to the stopping power of low-energy hydrogen beams passing through helium. Phys. Rev. **A49**, 603-606.

[74] Papaconstantopoulos DA (1986) Handbook of the Band Structure of Elemental Solids. Plenum Press, New York.

[75] Reinhold CO, Burgdörfer J, Kemmler J, Koschar P (1992) Simulation of convoy-electron emission. Phys. Rev. **A45**, R2655-R2658.

[76] Reinhold CO, Burgdörfer J, Kimura K, Mannami M (1994) Rainbow scattering of convoy electrons near surfaces. Phys. Rev. Lett. **73**, 2508-2511.

[77] Ridder D, Schneider D (1982) Auger spectra excited in collisions of fast phosphorus ions with thin carbon foils. Phys. Rev. **A25**, 921-930.

[78] Ritchie RH (1991) Electron spectra in solids. In: Interaction of Charged Particles with Solids and Surfaces. NATO Advanced Science Institutes Series B271. Gras-Marti A, Urbassek HM, Arista NR, Flores F (eds.). Plenum Press. pp. 197-225.

[79] Ritchie RH, Claussen C (1982) A core plasma model of charged particle track formation in insulators. Nucl. Instr. Meth. **B198**, 133-138.

[80] Ritchie RH, Brandt W, Echenique PM (1976) Wake potential of swift ions in solids. Phys. Rev. **B14**, 4808-4812.

[81] Rösler M, Brauer W (1991) Theory of electron emission from nearly-free-electron metals by proton and electron bombardment. In: Particle Induced Electron Emission I. Vol. 122. Springer Tracts of Modern Physics. Springer Verlag. pp. 1-66.

[82] Rothard H (1995) Swift heavy ion induced electron emission from solids. Scanning Microsc. **9**, 1-42.

[83] Rothard H, Schou J, Groeneveld KO (1992) Projectile- and charge-state-dependent electron yields from ion penetration of solids as a probe of preequilibrium stopping power. Phys. Rev. **A45**, 1701-1710.

[84] Rothard H, Caraby C, Cassimi A, Gervais B, Grandin JP, Jardin P, Jung M, Billebaud A, Chevallier M, Groeneveld KO, Maier R (1995) Target-thickness-dependent electron emission from carbon foils bombarded with swift highly charged heavy ions. Phys. Rev. **A51**, 3066-3078.

[85] Rozet J, Chetioui A, Bouisset P, Vernhet D, Wohrer K, Touati A, Stephan C, Grandin JP (1987) Anomalous population of deep capture states of fast ions emerging from solid foils. Phys. Rev. Lett. **58**, 337-340.

[86] Rozet JP, Chetioui A, Piquemal P, Vernhet D, Wohrer K, Stéphan C, Tassan-Got L (1989) Charge-state distributions of few-electron ions deduced from atomic cross sections. J. Phys. B: At. Mol. Opt. Phys. **22**, 33-48.

[87] Ryufuku H, Watanabe T (1978) Charge transfer in collisions of atomic hydrogen with O^{8+}, He^{2+}, and H^{+}. Phys. Rev. **A18**, 2005-2015.

[88] Ryufuku H, Watanabe T (1979) Charge transfer cross section for collisions of Li^{3+}, Be^{4+}, B^{5+}, and C^{6+} ions with atomic hydrogen. Phys. Rev. **A19**, 1538-1549.

[89] Salin A (1969) Ionization of atomic hydrogen by proton impact. J. Phys. B: Atom. Molec. Phys. **2**, 631-639.

[90] Schiwietz G (1990a) Population of projectile-ion states during the passage of high energy Ne-ions through thin carbon foils. Radiat. Effects Defects Solids **112**, 195-200.

[91] Schiwietz G (1990b) Coupled-channel calculation of stopping powers for intermediate-energy light ions penetrating atomic H and He targets. Phys. Rev. **A42**, 296-306.

[92] Schiwietz G (1992) Electron ejection induced by fast projectiles. In: Ionization of Solids by Heavy Particles. Baragiola R (ed.). NATO Advanced Study Institutes Series 306. Plenum Press, New York. pp. 197-214.

[93] Schiwietz G, Fritsch W (1987) Determination of differential cross sections in classical trajectory Monte Carlo calculations. J. Phys. **B20**, 5463-5474.

[94] Schiwietz G, Grande PL (1994a) Electronic stopping based on atomic and solid-state wavefunctions, Rad. Eff. Def. Solids **130/131**, 137-156.

[95] Schiwietz G, Grande PL (1994b) On the treatment of light-ion electronic stopping in dense matter. Nucl. Instr. Meth. **B90**, 10-19.

[96] Schiwietz G, Xiao G (1996) Electron ejection from

solids induced by fast highly-charged ions. Nucl. Instr. Meth. Phys. Res. **B107**, 113-127.

[97] Schiwietz G, Schneider D, Tanis J (1987) Formation of Rydberg states in fast ions penetrating thin carbon-foil and gas target. Phys. Rev. Lett. **59**, 1561-1564.

[98] Schiwietz G, Schneider D, Biersack JP, Stolterfoht N, Fink D, Mattis A, Skogvall B, Altevogt H, Montemayor V, Stettner U (1988) Cascade-induced asymmetry in Auger-electron emission following fast ion-solid interactions. Phys. Rev. Lett. **61**, 2667-2680.

[99] Schiwietz G, Biersack JP, Schneider D, Stolterfoht N, Fink D, Montemayor V, Skogvall B (1990) Investigation of δ-electron emission in collisions of highly charged fast Ne projectiles with carbon-foil targets. Phys. Rev. **B41**, 6262-6271.

[100] Schiwietz G, Grande PL, Skogvall B, Biersack JP, Köhrbrück R, Sommer K, Schmoldt A, Goppelt P, Kádár I, Ricz S, Stettner U (1992) Influence of nuclear track potentials in insulators on the emission of target Auger electrons. Phys. Rev. Lett. **69**, 628-631.

[101] Schiwietz G, Grande PL, Auth C, Winter H, Salin A (1994) Angular dependence of energy loss in proton-helium collisions. Phys. Rev. Lett. **72**, 2159-2162.

[102] Schneider D, Bruch R, Schwarz WHE, Chang TC, Moore CF (1977) Identifications of Auger spectra from 2-MeV foil-excited carbon ions. Phys. Rev. **A15**, 926-934.

[103] Schneider D, Zeitz W, Kowallik R, Schiwietz G, Schneider T, Stolterfoht N, Wille U (1986) Effects of external electric fields on high Rydberg states formed in foil and gas interactions of 85 MeV Ne^{6+} ions. Phys. Rev. **A34**, 169-175.

[104] Schneider D, Schiwietz G, DeWitt D (1993) Doubly differential secondary-electron yields following 8 MeV/u U^{68+} and 3.5 MeV/u U^{38+} ion impact on a thin carbon-foil target. Phys. Rev. **A47**, 3945-3950.

[105] Schou J (1980) Transport theory for kinetic emission of secondary electrons from solids. Phys. Rev. **B22**, 2141-2174.

[106] Sigmund P, Tougaard S (1981) Electron emission from solids during ion bombardment. Theoretical aspects. In: Inelastic Particle-Surface Collisions. Springer Series in Chemical Physics 17. Taglauer E, Heiland W (eds.). Springer Verlag. pp. 2-37.

[107] Skogvall B, Schiwietz G (1990) Evidence for electron correlation in the two electron continuum during double ionization in 300-keV H^+ + He collisions. Phys. Rev. Lett. **65**, 3265-3268.

[108] Skogvall B, Schiwietz G (1992) Single and double ionization in 300-keV H^+ + He collision at small impact parameters. Phys. Rev. **A46**, 5687-5695.

[109] Spohr R (1990) Ion Tracks and Microtechnology. Vieweg Verlag, Braunschweig, Germany.

[110] Sternglass EJ (1957) Theory of secondary electron emission by high-speed ions. Phys. Rev. **108**, 1-12.

[111] Stolterfoht N (1971) Angular and energy distribution of electrons produced by 200-500 keV protons in gases. Z. Phys. **248**, 81-100.

[112] Stolterfoht N (1987) High resolution Auger spectroscopy in energetic ion atom collision. Phys. Rep. **146**, 315-424.

[113] Stolterfoht N, Schneider D, Burch D, Wieman H, Risley JS (1974) Mechanisms for electron production in 30-MeV O^{n+} + O_2 collisions. Phys. Rev. Lett. **33**, 59-62.

[114] Teillet-Billy D, Gauyacq JP (1990) Position and width of a negative ion state in front of a surface: formation of $C^-(^4S)$ ions by electron capture. Surf. Science **239**, 343-352.

[115] Vriens L (1969) Binary-encounter and classical collision theories. In: Case Studies in Atomic Physics. Vol. 1. McDaniel EW, McDowell MRC (eds.). North-Holland, Amsterdam, The Netherlands. pp. 335-398.

[116] Wang ZG, Dufour C, Paumier E, Toulemonde M (1994) The Se sensitivity of metals under swift-heavy-ion irradiation: A transient thermal process. J. Phys.: Condens. Matter **6**, 6733-6750.

[117] Watson CC, Tombrello TA (1985) A modified lattice potential model of electronically mediated sputtering. Radiation Effects **89**, 263-283.

[118] Wien K, Koch Ch, Nguyen van Tau (1995) Line shifts in mass spectra of secondary ions ejected from solids by MeV-ion impact. Nucl. Instr. Meth. **B100**, 322-330.

[119] Wille U (1983) Direct ionisation of the 4fσ molecular orbital in slow ion-atom collisions. J. Phys. **B16**, L275-L279.

[120] Wilson WE, Toburen LH (1973) Electron emission in H_2^+-H_2 collisions from 0.6 to 1.5 MeV. Phys. Rev. **A7**, 1535-1544.

[121] Xiao G, Schiwietz G, Grande PL, Schmoldt A, Grether M, Köhrbrück R, Stolterfoht N, Spieler A, Stettner U (1996) Evidence for convoy-electron shifts due to induced potentials. Nucl. Instr. Meth. **B115**, 215-219.

[122] Yamazaki Y, Stolterfoht N, Miller PD, Krause HF, Pepmiller PL, Datz S, Sellin IA, Scheurer JN, Andriamonje A, Bertault D, Chemin JF (1988) Angular momentum distributions of autoionizing states produced by 1.5-5 MeV C^+ ions in carbon foils. Phys. Rev. Lett. **61**, 2913-2916.

[123] Ziegler JF, Biersack JP, Littmark U (1985) The Stopping and Range of Ions in Solids. Pergamon, New York.

Discussion with Reviewers

R. Baragiola: You mention Coulomb explosions and thermal spikes as the two ways to convert electronic excitations into

the atomic motion needed for material modification. How likely are those mechanisms compared to direct excitation or dissociation in single events? These direct mechanisms cause chemical changes like decoloration and decomposition even for impact of ultraviolet light, and weakly ionizing electrons and protons.

Authors: For small projectile charges and also for single-photon excitation, we expect Coulomb explosion and thermal spike to be of no importance. For heavy projectiles, however, both mechanisms may strongly exceed the material modification rates due to direct mechanisms. In fact, for polypropylene, we have observed a threshold effect in the carbonization rate (foil thickness changes) for projectile charges near $Z_p = 10$. For this material, we see no indication for direct mechanisms (which should yield a Z_p^2 scaling). It is noted that the situation is different for other materials; there are even polymers which do not show any threshold effect in the carbonization rate.

R. Baragiola: In the discussion of convoy electrons, you consider the image interaction with the surface but not the Coulomb interaction with the many low energy secondary electrons ejected by the same ion, which may be of comparable magnitude. What do you think would be the effect of the space charge created by these low energy electrons?

Authors: For heavy projectiles, we expect the number of ejected low energy secondary electrons near the track (about 15% of the total electron yield) to exceed the projectile image charge. The corresponding space-charge potential, however, will be reduced by a factor $v_p/4v_e$ due to the image potential of the ejected electrons. Thus, we estimate a 40% contribution to the total potential for Ag^{37+} projectiles and less then 10% for N^{7+} projectiles. Unfortunately, there seems to be no quantitative model for the total dynamic potential that includes the space-charge effect.

R.H. Ritchie: A question that might be addressed by the authors has to do with their theoretical model of electron transport following ejection from an atomic site by a high Z-ion. It is stated that such electrons are assumed to slow down continuously (the "csda") until they come to rest. How are they treated following this? The central track region becomes highly charged according to the results displayed in Figure 2; it is conceivable that very strong acceleration toward the center of the track, and even avalanche formation, could take place after electrons are stopped in the solid.

Authors: In contrast to the electron-gas picture, we assume these electrons to be trapped and to stay at rest. Of course, this assumption can only be valid for particular materials (insulators). The acceleration toward the center of the track may give rise to an avalanche, but the field can also stabilize trapped electrons. Our experimental results for polypropylene as well as earlier measurements with mylar targets, however, point to existence of long-lived traps for these materials.